

RESEARCH ARTICLE

A Semiparametric Generalized Exponential Regression Model with a Principled Distance-based Prior for Analyzing Trends in Rainfall

Arijit Dey and Arnab Hazra

Department of Mathematics and Statistics, Indian Institute of Technology Kanpur, Kanpur, 208016, India.

ARTICLE HISTORY

Compiled September 7, 2023

ABSTRACT

The Western Ghats mountain range holds critical importance in regulating monsoon rainfall across Southern India, with a profound impact on regional agriculture. Here, we analyze daily wet-day rainfall data for the monsoon months between 1901–2022 for the Northern, Middle, and Southern Western Ghats regions. Motivated by an exploratory data analysis, we introduce a semiparametric Bayesian generalized exponential (GE) regression model; despite the underlying GE distribution assumption being well-known in the literature, including in the context of rainfall analysis, no research explored it in a regression setting, as of our knowledge. Our proposed approach involves modeling the GE rate parameter within a generalized additive model framework. An important feature is the integration of a principled distance-based prior for the GE shape parameter; this allows the model to shrink to an exponential regression model that retains the advantages of the exponential family. We draw inferences using the Markov chain Monte Carlo algorithm. Extensive simulations demonstrate that the proposed model outperforms simpler alternatives. Applying the model to analyze the rainfall data over 122 years provides insights into model parameters, temporal patterns, and the impact of climate change. We observe a significant decreasing trend in wet-day rainfall for the Southern Western Ghats region.

KEYWORDS

Climate change; Generalized exponential distribution; Markov chain Monte Carlo; Penalized complexity prior; Semiparametric Bayesian regression; Western Ghats; Wet-day precipitation modeling

1. Introduction

The Western Ghats, a prominent mountain range along the western coast of India, plays a crucial role in shaping the climatic patterns and hydrological dynamics of Southern India. Known for its exceptional biodiversity, lush forests, and vital water resources, the Western Ghats has long captured the attention of researchers and environmentalists [32, 50]. Among the various climatic parameters that influence this ecologically significant region, rainfall is a crucial driver of its diverse ecosystems, water availability, and overall environmental health. The Western Ghats, characterized by its rugged terrain and proximity to the Arabian Sea, experiences a unique and intricate rainfall pattern heavily influenced by monsoon dynamics [48]. Over the last century,

this region has experienced notable climatic shifts due to global climate change and local human activities [1, 49]. Analyzing wet-day rainfall in this region during monsoon months over an extended period of 122 years using a flexible statistical model offers a valuable opportunity to gain insights into long-term trends, variability, and potential shifts in the monsoonal regime.

Researchers have widely employed the exponential distribution to model rainfall data [16, 46] in literature; its simplicity integrates seamlessly into hydrological and climatological frameworks. However, contemporary research increasingly recognizes the need for innovative probability distribution models for better encompassing complex real-world data patterns. This realization has prompted the introduction of novel probability classes with far-reaching implications across diverse research domains. [2] provides an excellent overview of newly developed distributions. A notable collection of models are generalized distributions, gaining attention from both practical and theoretical statisticians for their adaptability to various datasets. Some examples include the Marshall-Olkin generalized exponential distribution [31], generalized inverse Gaussian distribution [21], generalized Rayleigh distribution [26], etc. A more comprehensive examination of these distributions is available in [45].

[10] introduced another crucial generalized distribution called the generalized exponential (GE) distribution, which emerges as a specific case within the three-parameter exponentiated-Weibull model. The GE distribution has two parameters- a shape and a rate (or scale, defined as the inverse of rate) parameter. This distribution boils down to an exponential distribution when the shape parameter is one. Thus, with an additional shape parameter, it expands the capabilities of the exponential distribution, making it more adaptable to various datasets. Since its introduction, many researchers have integrated substantial advancements in exploring different properties, estimation strategies, extensions, and applications of this distribution. For instance, [11] found the efficacy of GE distribution compared to gamma or Weibull distributions, whereas [12] discussed different methods of estimating the parameters of GE distribution. [20], [38], and [25] explored Bayesian estimation and prediction methods in this context. [13] reviewed the existing results and discussed some new estimation methods and their characteristics. Numerous researchers have modeled the experimental data using GE distribution across several disciplines like meteorological studies [15, 29]; flood frequency analysis [30]; reliability analysis [3]; lifetime analysis [4]; risk analysis [42]. But, as of our knowledge, any GE regression-type model has never been proposed in the literature. In this study, taking a step beyond exponential regression, we employ the GE regression framework to explore rainfall patterns.

Rainfall data collected over a century are inherently nonstationary. Here, modeling the temporal trend using traditional parametric regression would struggle to capture the intricate and evolving short-term temporal patterns. In this context, a semiparametric regression setup emerges as a promising approach. In the existing literature, many researchers have delved into applying semiparametric regression techniques for analyzing rainfall patterns [34, 53]. While a generalized linear model (GLM) assumes the link function to be a linear combination of the covariates, the more flexible generalized additive models [GAM, 14] allow the link function to be a sum of nonlinear smooth functional forms of the underlying covariates. We generally model each smooth function in GAMs as a linear combination of basis functions like cubic B-splines. Instead of estimating the entirely unknown function, we draw inferences based on basis function coefficients [8]. Henceforth, instead of GAM, we use the term ‘semiparametric regression’, which is common in Bayesian nonparametrics. The rate parameter of the GE distribution is always positive, and hence, it would be reasonable to model the

log-rate in a semiparametric regression framework.

Within the Bayesian methodology, priors hold a pivotal role in inference, and the literature provides a diverse spectrum of prior distributions utilized for regression coefficients in semiparametric regression frameworks. For instance, Gaussian prior was employed by [7], while [27] opted for Laplace prior. [28] utilized Zellner’s g -prior, while [6] considered flat priors, and [23] used the Normal-Gamma prior. On the other hand, the gamma distribution has consistently been considered the most natural prior choice for the shape parameter of the GE distribution; authors who introduced the GE distribution chose a gamma prior for the shape parameter in [25] as well. Besides [38] and [22] also employed gamma prior for the shape parameter. However, the literature demonstrates that a handful of alternative prior choices have also been utilized. For example, [33] employed a Jeffrey’s prior, indicating their preference for an objective prior, and [5] opted for a non-informative prior in their study.

The Penalized Complexity (PC) prior, introduced by [43], has emerged in recent literature, which mitigates the model complexity through penalization. In cases where a model extends from a simpler foundational model by incorporating an additional parameter, this type of prior becomes applicable; it penalizes the escalation in model complexity that arises when favoring the extended model over its more straightforward counterpart. Existing literature encompasses instances of this approach across various models [47]. [51] developed PC priors for estimating the effective degrees of freedom in Bayesian penalized splines (P-splines), while [35] discussed a PC prior for the skewness parameter of the power links family, and [44] proposed interpretable and comprehensive PC priors for the coefficients of a stationary autoregressive process.

In this paper, along with modeling the wet-day rainfall of the Western Ghats region for the last century by a semiparametric Bayesian GE regression model, we employ the PC prior for the GE shape parameter, which allows the GE regression to shrink towards an exponential regression. Thus, the exponential distribution is considered the base model for the GE distribution. In several practical examples [16, 17], the exponential distribution is already a reasonable model and enjoys several benefits of being a member of the exponential family, thus shrinking the GE distribution to its base model through shrinking the shape parameter to one is justified. On the other hand, we opt for the independent Gaussian priors for the regression coefficients. We draw inferences using the Markov chain Monte Carlo (MCMC) algorithm; here, conjugate priors are not available for the model parameters, and thus we update them using Metropolis-Hastings steps. We conduct a thorough simulation study by simulating 1000 datasets from each combination of the model generating and model fitting scenarios, and we compare the performances of parametric and semiparametric Bayesian GE regression models under the conventional gamma prior choices for the GE shape parameter along with our proposed one. We study the coverage probabilities for the shape parameter and the rate functions and compare these two models using widely applicable information criterion [WAIC, 52]. We implement the proposed methodology to the daily wet-day precipitation spanning from 1901 to 2022 in different regions of the Western Ghats mountain range, using the year as a covariate and wet-day precipitation as a response. We study the convergence and mixing of the MCMC chains and compare different model fits in terms of WAIC.

The paper is structured as follows: Section [2] delves into the GE distribution, thoroughly examining its properties. Section [3] discusses an exploratory data analysis that justifies our semiparametric GE model assumption for the wet-day precipitation data. In Section [4], we introduce the GE regression model. Proceeding to Section [5], we concentrate on delineating the prior specifications for the regression model,

including introducing a principled distance-based prior for the shape parameter of the GE distribution. Bayesian parameter inference is addressed in Section [6]. Section [7] presents the outcomes of the simulation study, while Section [8] discusses the results obtained from our proposed model and some simpler alternatives. Finally, Section [9] summarizes our findings and contributions.

2. Background: Generalized Exponential (GE) Distribution

We say a random variable X follows GE distribution if its cumulative distribution function (CDF) is given by

$$F(x; \alpha, \lambda) = \left(1 - e^{-\lambda x}\right)^\alpha; \quad x, \alpha, \lambda > 0,$$

where α is the shape parameter and λ is the rate parameter. The corresponding probability density function (PDF) is given by

$$f(x; \alpha, \lambda) = \alpha \lambda \left(1 - e^{-\lambda x}\right)^{\alpha-1} e^{-\lambda x}; \quad x, \alpha, \lambda > 0. \quad (1)$$

The GE distribution is a more complex model than the exponential distribution, as it incorporates an extra shape parameter. Both models coincide when $\alpha = 1$.

2.1. Properties of GE

The hazard function of the GE distribution is given by

$$h(x; \alpha, \lambda) = \frac{f(x; \alpha, \lambda)}{1 - F(x; \alpha, \lambda)} = \frac{\alpha \lambda \left(1 - e^{-\lambda x}\right)^{\alpha-1} e^{-\lambda x}}{1 - \left(1 - e^{-\lambda x}\right)^\alpha}; \quad x > 0.$$

The GE distribution has an increasing or decreasing hazard rate depending on the value of the shape parameter. The hazard function is decreasing for $\alpha < 1$, constant for $\alpha = 1$, and increasing for $\alpha > 1$. The moment generating function (MGF) of the GE distribution is given by

$$M_X(t) = \frac{\Gamma(\alpha + 1)\Gamma\left(1 - \frac{t}{\lambda}\right)}{\Gamma\left(1 + \alpha - \frac{t}{\lambda}\right)}; \quad 0 \leq t < \lambda,$$

and differentiating the log of the MGF with respect to t repeatedly and then setting $t = 0$, we get the expectation, variance, and skewness of GE distribution as

$$\begin{aligned} \mathbf{E}(X) &= \lambda^{-1} [\psi(\alpha + 1) - \psi(1)], \\ \mathbf{V}(X) &= \lambda^{-2} \left[\psi^{(1)}(1) - \psi^{(1)}(\alpha + 1) \right], \\ \text{Skewness}(X) &= \left[\psi^{(2)}(\alpha + 1) - \psi^{(2)}(1) \right] / \left[\psi^{(1)}(1) - \psi^{(1)}(\alpha + 1) \right]^{\frac{3}{2}}, \end{aligned}$$

where $\psi^{(m)}(z) = \frac{\partial^m}{\partial z^m} \psi(z) = \frac{\partial^{m+1}}{\partial z^{m+1}} \ln \Gamma(z)$ is the polygamma function of order m ; for $m = 0$, it denotes the digamma function.

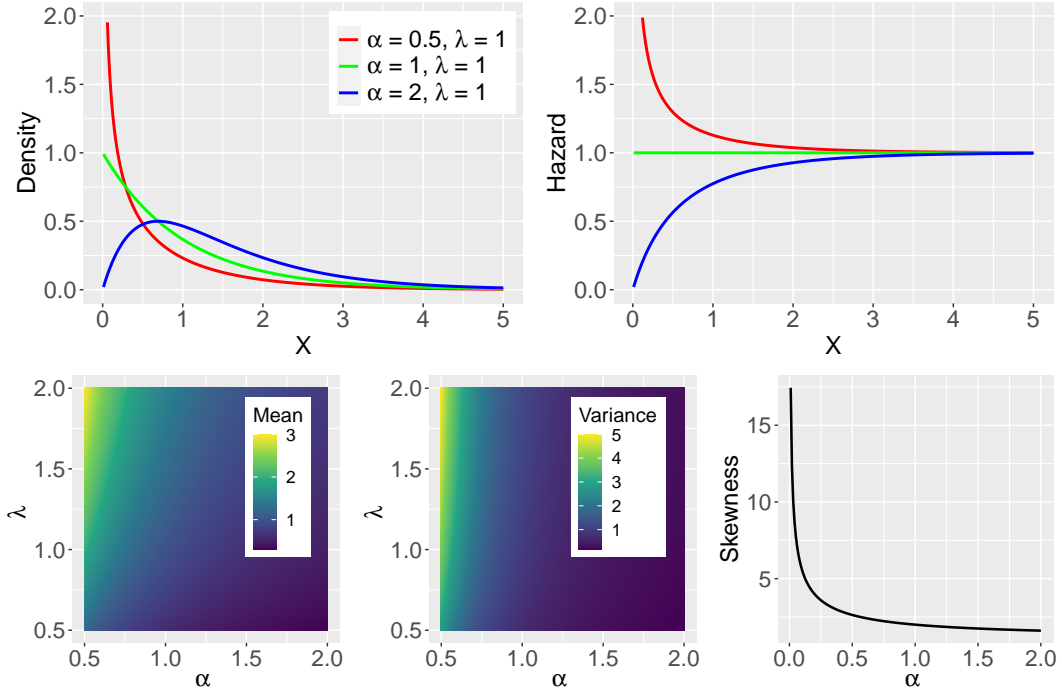


Figure 1. Generalized Exponential probability density function (top-left), hazard function (top-right), mean (bottom-left), variance (bottom-middle), and skewness (bottom-right) functions. Both top panels share the same legend.

Figure 1 sheds light on different aspects of the GE distribution, e.g., PDF, hazard function, mean, variance, and skewness. The top-left panel of Figure 1 shows that for $\alpha < 1$, the curve depicting the PDF of the GE distribution has an asymptote at the Y-axis and then decreases exponentially and monotonically as we move across the positive real line. With $\alpha = 1$, GE coincides with the exponential distribution, thus having mode at zero (with value = λ) and gradually decreasing similarly as the previous case. When $\alpha > 1$, the curve initiates at zero, then increases over a range of values, and eventually decreases monotonically, having a unique mode at $\log(\alpha)/\lambda$. As mentioned earlier, the top-right panel of Figure 1 shows that the hazard function is monotonically increasing when $\alpha < 0$, monotonically decreasing when $\alpha > 0$, and constant (the value being $\lambda = 1$) when $\alpha = 1$. The mean and variance of GE behave somewhat in a similar manner. From the bottom-left and the bottom-middle panel of Figure 1, we see for a fixed value of α , both mean and variance decrease with increasing λ and for a fixed value of λ , both increase as α increases. On the other hand, the skewness of the GE distribution depends only on the shape parameter and decreases exponentially with increasing α (bottom-right panel of Figure 1).

3. Data Preprocessing and Exploratory Data Analysis

In this section, we describe the preprocessing steps involved in obtaining the dataset comprising average daily precipitation data for rainy days in the Northern, Middle, and Southern Western Ghats regions during the monsoon months between 1901–2022. Besides, we discuss pieces of evidence based on exploratory data analysis that confirm the suitability of a GE distribution for fitting the data and to determine whether a semiparametric mean structure is necessary or a linear trend structure would suffice.

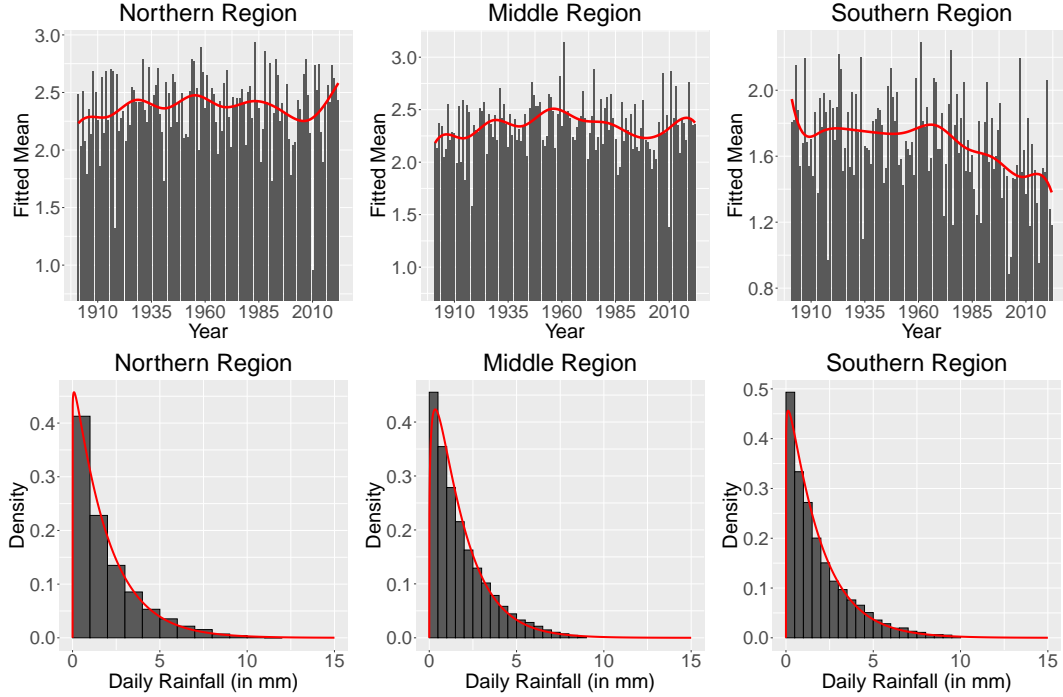


Figure 2. Bar diagrams of the annual average wet-day rainfall during June through September along with fitted mean curves based on twelve cubic B-splines with equidistant knots, for Northern, Middle, and Southern Western Ghats regions (top panels). Histograms of the detrended residuals from the daily rainfall overlapped with the fitted GE densities (bottom panels).

We obtain daily gridded rainfall (in mm) data over the Western Ghats region with a spatial resolution of $1.0^\circ \times 1.0^\circ$, covering the period from 1901–2022. The data was sourced from the official website of the Indian Meteorological Department, Pune (https://www.imdpune.gov.in/cmpg/Griddata/Rainfall_1_NetCDF.html). The gridded data product was obtained through spatial interpolation of ground-station data following the procedure described in [36]. We extract the daily rainfall information for June, July, August, and September (JJAS) throughout all the years. Additionally, we exclude days within the JJAS months where recorded rainfall amounts were zero. Out of the pixels representing the Western Ghats area, we group them into three distinct significant regions: the Northern, Middle, and Southern regions (the regions are shown in the supplementary material). We compute the daily rainfall values for each region by calculating the average of the corresponding pixel values within that region. Afterward, we conduct a further analysis based on these regions.

Given our dataset (after preprocessing) spans over a century, our initial focus involves performing necessary analyses to address any potential trends within the data. In the top panels of Figure 2, we present a bar diagram depicting the average yearly rainfall for each year. No clear long-term linear trend is observable for any of the three regions. However, several short-term upward and downward patterns are noticeable. We use a basis spline regression approach to explore such short-term trends, which treats daily rainfall values as response variables and corresponding years as covariates. Considering the residuals from this regression, we can effectively eliminate any potential trends embedded in the data. We overlap the estimated means with the bar diagrams in the top panels of Figure 2. Firstly, the estimated mean curve aligns well with the visualized bar diagram. Moreover, both components highlight the presence

of a nonstationary rainfall pattern. This pattern, in turn, underscores the suitability of employing a semiparametric regression model, which can effectively accommodate and incorporate these nonstationary patterns within the data.

Subsequently, after conducting a fundamental analysis to identify and remove outliers via the popular adjusted-boxplot method developed by [19], we present two important visualizations in the bottom panels of Figure 2, where the panels correspond to three regions of interest. Firstly, we showcase a histogram illustrating the distribution of the detrended residuals obtained by exponentiating the residuals obtained by fitting a semiparametric regression curve to the log-transformed wet-day rainfall observations, which aligns with the standard link function formulations for generalized additive models. Additionally, a red line denotes the fitted density of the GE distribution, with parameters estimated from the detrended residuals. We observe a strong alignment between the estimated density and the associated histograms, indicating a favorable fit. This visual representation significantly supports the rationale behind the GE regression model proposed in this paper. Additionally, the plots highlight a marked convergence of the GE distributions towards their foundational model, the exponential distribution. This convergence also reinforces our second consideration: using a novel distance-based prior for the shape parameter of the GE distribution.

4. Generalized Exponential (GE) Regression

The GE regression model is a statistical model that we can use for modeling continuous positive-valued response variables. It can be considered an extension of the standard linear regression model that allows for non-Gaussian and asymmetric distributions, accommodating heteroscedasticity and skewness in the data. The regression framework assumes that the response variable Y follows a GE distribution, and it models the relationship between the Y and the covariates $\mathbf{X} = (X_1, \dots, X_P)'$ through a linear predictor η . The linear predictor is a linear combination of the covariates with associated regression coefficients, given as

$$\eta(\mathbf{X}) = \beta_0 + \beta_1 X_1 + \beta_2 X_2 + \dots + \beta_P X_P, \quad (2)$$

where $\boldsymbol{\beta} = (\beta_0, \beta_1, \dots, \beta_P)'$ is the vector of regression coefficients.

In the GE regression model, the shape parameter α is considered an inherent property of the distribution that characterizes the shape and asymmetry of the distribution, allowing for a more flexible modeling approach compared to a standard linear regression with a Gaussian error component. On the other hand, the rate parameter λ is the parameter of interest in the regression model, which captures the association between the covariates and the response variable. By incorporating the covariates through the rate parameter, the model captures how changes in the covariate values influence the rate or dispersion of the response variable. Moreover, given that the rate parameter of the GE distribution is positive, we relate it to the linear predictor from (2) using a link function, which is designed to ensure the rate parameter always stays positive. Thus, we can conceptualize the GE Regression model as

$$Y_i | \mathbf{X}_i = \mathbf{x}_i \sim GE(\alpha, \lambda_i),$$

where $g(\lambda_i) = \eta(\mathbf{x}_i)$, with $g(\cdot)$ representing the appropriate link function and $\mathbf{x}_i = (x_{i1}, x_{i2}, \dots, x_{iP})'$. The parameters in the Generalized Exponential regression model,

including the regression coefficients and the shape parameter, are typically estimated using maximum likelihood estimation or other suitable estimation methods.

The above-explained theory introduces a parametric framework for the GE regression model, aiming to capture the relationship between the response variables and the covariates by utilizing rate parameters. However, this paper adopts a semiparametric approach to achieve the same objective, which allows us to incorporate both parametric and nonparametric components into the model, providing flexibility and accommodating potential complexities in the relationship between the covariates and the response variables. We introduce the specific form of the predictor function and other essential formulations following a general introduction to semiparametric regression models.

4.1. Semiparametric Regression

Parametric regression assumes a known distribution for the response variable and estimates a finite-dimensional set of parameters. It is straightforward, provides easy estimation, and offers interpretability. However, it may struggle to capture nuanced aspects of the data, such as non-linearity or variable interactions. In contrast, nonparametric regression assumes no specific form for the relationship between the response and explanatory variables, allowing flexibility based on data-derived information. While this approach allows for more flexible modeling, it is computationally intensive, less interpretable, and can be affected by the *curse of dimensionality*. Semiparametric regression integrates the above two approaches, allowing us to have the best of both regimes. It incorporates the interpretability of the parametric setup and flexibility of the nonparametric setup.

In linear or generalized linear models (GLM) that fall under the parametric setup, we assume the conditional mean of the distribution of the response variable is linked with the linear predictor through a linear combination of the covariates or their functions. Semiparametric setup extends this domain of regression models by introducing the nonparametric component in the linear predictors. In this setup, the most general formulation of the linear predictor can be given as

$$\eta(\mathbf{x}) = \sum_{p=1}^P f_p(x_p), \quad (3)$$

where f_j 's are smoothing functions of continuous covariates and $\mathbf{x} = (x_1, x_2, \dots, x_P)'$. Regarding smoothing functions, most semiparametric methods assume they can be expressed as a linear combination of finite basis functions, often denoted as

$$f_p(z) = \sum_{k=1}^{K_p} \beta_{p,k} B_{p,k}(z); \quad p = 1, 2, \dots, P, \quad (4)$$

where $B_{p,k}(\cdot)$'s are known basis functions and $\beta_{p,k}$ are unknown basis function coefficients that determine the shape of the smoothing function $f_p(z)$. A basis expansion of M terms can match the true curve $f_p(\cdot)$ at any M points X_1, \dots, X_M in the range of covariates. Hence, increasing M gives us an arbitrarily flexible model.

In this study, we employ a semiparametric model akin to (3) for the rate parameter of the GE distribution. With a covariate vector comprising P components and the

appropriate logarithmic link function, the regression model takes the form:

$$Y_i | \mathbf{X}_i = \mathbf{x}_i \sim GE(\alpha, \lambda(\mathbf{x}_i)) \text{ with } \log \{\lambda(\mathbf{x}_i)\} = \sum_{p=1}^P \sum_{k=1}^{K_p} \beta_{p,k} B_{p,k}(x_{ip}), \quad (5)$$

where $B_{p,k}(\cdot)$'s are cubic B-splines and $\beta_{p,k}$'s are the spline coefficients representing the weights assigned to the corresponding spline functions. To provide a brief overview, a cubic B-spline is a piecewise-defined polynomial cubic function that is defined on a set of knots or control points, taking the form $B_s(x) = (x - v_s)_+^3$ where v_s 's are the fixed knots that span the range of x and '+' denotes the positive part.

5. Prior Specification

Selecting an appropriate prior is one of the most crucial parts of a Bayesian analysis. While there is no universal rule for constructing optimal prior distribution, choosing an appropriate prior can significantly enhance the quality of the study. A well-chosen proper prior can stabilize the posterior distribution and yield better results compared to an improper prior [Chapter 4, 39]. This section defines the prior distribution parameters of the regression model presented in (5).

In semiparametric Bayesian regression, instead of formulating an explicit prior distribution for λ , independent prior distributions are explicitly specified for the spline coefficients $\boldsymbol{\beta} = (\beta_1, \beta_2, \dots, \beta_K)'$. This paper considers independent weakly-informative Gaussian priors for β_k 's. As for the shape parameter of the GE distribution, we employ a newly developed class of priors. In cases where a model is constructed based on a simpler base model, the chosen prior should accurately reflect the characteristics of the model considered and capture its departure from the base model. This type of prior construction is founded upon the work of [43], who introduced the Penalized Complexity (PC) prior. The PC prior is a model-based prior that imposes a penalty on the deviation of the model of consideration from its simpler base version at a logarithmic constant rate. The following subsections discuss the PC prior for α .

5.1. Penalized Complexity (PC) prior

The PC prior is an informative proper prior that exhibits robustness properties of high quality and invariance under reparameterization. It aims to penalize the complexity that arises when we move from a simpler base model to a more complex one, thereby preventing overfitting and adhering to *Occam's razor principle* [43]. By using the PC prior, we uphold the *principle of parsimony*, which suggests a preference for simpler models until sufficient evidence supports more complex alternatives.

The PC prior is established based on the statistical difference between the proposed complex model and its base model. We quantify this distance using the Kullback-Leibler divergence (KLD) [24]. KLD is an information-based measure that essentially measures how much information we lose when we substitute a complex model having PDF f with its simpler version having PDF g . For the GE distribution, the exponential distribution is commonly selected as the appropriate base model. Hence, for our purposes, we consider f as the GE PDF and g as the exponential PDF.

For two continuous distributions with PDF f and g defined over the same support,

KLD is defined as

$$\text{KLD}(f \parallel g) = \int_{-\infty}^{\infty} f(y) \log \left(\frac{f(y)}{g(y)} \right) dy. \quad (6)$$

We define the distance between the two models by the ‘unidirectional’ distance function $d(f \parallel g) = \sqrt{2\text{KLD}(f \parallel g)}$ [43]. The absence of symmetry in KLD is not a concern within this context. Our main focus is on quantifying the additional complexity that arises from employing the intricate model rather than the other way around.

The main idea of the PC prior involves assigning priors to the distance between two models, $d(\alpha)$, rather than directly on the model parameters, and then by employing a change-of-variables approach, one can obtain a prior distribution for the parameter of interest. While constructing the PC prior for the shape parameter α , we take this distance as a function of α , i.e., $d(\alpha) = \sqrt{2\text{KLD}(\alpha)} = \sqrt{2\text{KLD}(f \parallel g)}$ with f and g being GE and exponential PDFs respectively.

To incorporate the fact that the prior should have a decaying nature as a function of the distance between the two models, we take the constant rate penalization assumption and construct the PC prior by assigning an exponential prior to the distance, i.e., $d(\alpha) \sim \text{Exp}(\theta)$ with $\theta > 0$. This gives us the PC prior for α as

$$\pi(\alpha) = \theta e^{-\theta d(\alpha)} \left| \frac{\partial d(\alpha)}{\partial \alpha} \right|, \quad (7)$$

where $\theta > 0$ is a user-defined quantity that controls the prior mass at the tail. We impose this quantity in such a way that this characterizes how informative the PC prior we want. This is achieved by imposing a condition $\Pr[d(\alpha) > U] = \xi$ where U is the upper bound of the tail-event and ξ is the weight of the event [43].

5.2. PC prior for the shape parameter of GE distribution

This section contains the KLD between our complex model, the GE model (f) and its natural base model, Exponential (g), and the PC prior of the shape parameter, α .

Theorem 5.1. *The KLD, with f being the PDF of the GE distribution given in (1) and g being the PDF of the exponential distribution with rate λ , is given by*

$$\text{KLD}(\alpha) = \log(\alpha) + 1/\alpha - 1.$$

Theorem 5.2. *The PC prior for the shape parameter (α) of the Generalized Exponential (GE) distribution is supported over the positive real line and given as*

$$\pi(\alpha) = \frac{\theta}{2} \cdot \exp \left(-\theta \sqrt{2 \log(\alpha) + \frac{2(1-\alpha)}{\alpha}} \right) \cdot \left(2 \log(\alpha) + \frac{2(1-\alpha)}{\alpha} \right)^{-\frac{1}{2}} \cdot \left| \frac{1}{\alpha} - \frac{1}{\alpha^2} \right|.$$

Proof. Proof for Theorem 5.1 is given in the Appendix A and Theorem 5.2 follows directly from (7) and the expression $d(\alpha) = \sqrt{2\text{KLD}(\alpha)}$. Moreover, Theorem 5.2 includes a scaling factor which ensures that $\pi(\cdot)$ integrates to one. \square

In Figure 3 we illustrate $\pi(\alpha)$ for different hyperparameter specifications θ . We notice a proportional relationship between the value of θ and the extent of contraction

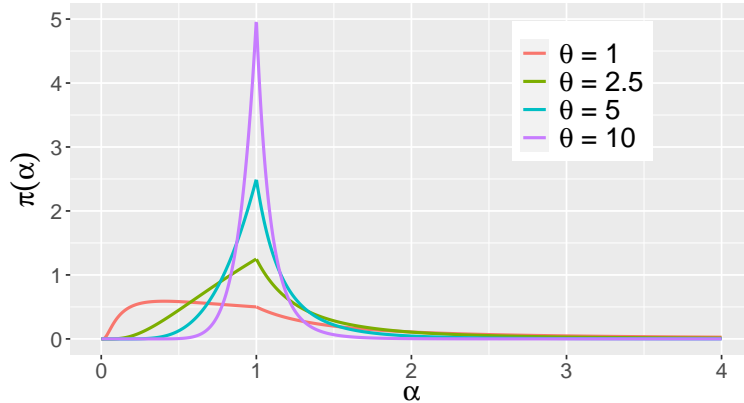


Figure 3. The PC prior for the shape parameter of the GE distribution for different choices of the hyperparameter θ .

to the base model. As the value of θ decreases, the tails become heavier, resulting in reduced contraction towards the base model. We also observe that for $\theta \leq 4/3$, the mode of the PDF occurs at a value of α less than one, but for $\theta \geq 4/3$, the mode is at $\alpha = 1$ (Figure 3). One might expect the prior would have mode at $\alpha = 1$ irrespective of the value of θ . Here, we do not necessarily need the mode at $\alpha = 1$, and rather we should rely on a prior that is consistent with the principles of PC prior.

6. Inference

This paper employs Bayesian estimation methods to infer and quantify the uncertainty surrounding the parameters of interest. Fundamentally, Bayesian inference encompasses amalgamating prior knowledge or beliefs (prior probability) regarding a particular event or hypothesis with evidence or data (likelihood) via the Bayes theorem and derives a revised or updated belief (posterior probability), which provides a more comprehensive understanding of the values of the parameters in question and their inherent uncertainty.

In our context, the likelihood function based on n observations from the GE distribution under the regression setting from (5) is given by

$$L(\alpha, \boldsymbol{\beta} | \mathbf{y}) = \prod_{i=1}^n f(y_i; \alpha, \lambda(\mathbf{x}_i)), \quad (8)$$

where $\mathbf{y} = (y_1, y_2, \dots, y_n)'$ is the observed data, $f(y; \alpha, \lambda)$ is the PDF of the GE distribution from (1) and $\lambda(\mathbf{x}_i)$ taking form as given in (5). Also, let $\pi(\alpha)$ and $\pi(\boldsymbol{\beta})$ denote the specified mutually independent priors for the parameters α and $\boldsymbol{\beta}$.

Combining the priors for shape parameter α and the regression coefficients $\boldsymbol{\beta}$, and the likelihood function as given in (8), we obtain the joint posterior distribution as $\pi(\alpha, \boldsymbol{\beta} | \mathbf{y}) \propto L(\alpha, \boldsymbol{\beta} | \mathbf{y}) \cdot \pi(\boldsymbol{\beta}) \cdot \pi(\alpha)$ from which Bayesian inference is facilitated. However, the explicit form of the marginal posterior density of the parameters is not analytically tractable, leading to employing simulation-based techniques such as Markov chain Monte Carlo (MCMC) methods or numerical approximation methods like Integrated Nested Laplace Approximations (INLA), introduced by [41]. In this paper, we employ MCMC techniques for parameter inference, specifically utilizing the adaptive

Metropolis-Hastings algorithm within Gibbs sampling. We iteratively adjust the variance of the proposal distribution within the chain so that the acceptance rate remains between 0.3 and 0.5. We initiate the MCMC chains with an initial value of 1 for α and the maximum likelihood estimate for β as calculated under $\alpha = 1$. Our approach employs an algorithm that updates one parameter at a time. Regarding computational resources, conducting the simulations outlined in Section 7, involving 144 different configurations, each with 1000 datasets, and employing an MCMC output of 10000 iterations, required nearly 8 hours to finalize. This computational task was carried out on a desktop system equipped with a Ryzen 9 5900x 12-core 24-threaded processor and 64GB of RAM. On average, the computation time for a single MCMC chain was around 1 second for the parametric setup (assuming $\log(\lambda)$ to be a simple linear function of year) using a simple linear regression model and approximately 3 seconds for our proposed semiparametric model.

Furthermore, it is feasible to describe the ultimate distribution of the posterior estimates for the parameters α and β . In this setting, the *Bernstein-von Mises* theorem outlines the shape of this asymptotic distribution, delineating how the parameters α and β behave as the sample size tends towards infinity. To gauge the level of uncertainty linked with these parameter estimations, we investigate the asymptotic variance of the parameters, which is encapsulated by the inverse of the information matrix. Additional elaboration can be found in the supplementary materials.

7. Simulation Study

We conducted an extensive simulation study to demonstrate the effectiveness of the PC prior and the proposed semiparametric model over a parametric model, where the GE rate parameter (in log scale) is modeled as a simple linear function of the covariate(s). We designed two separate simulation setups for this purpose. In the first setup, we compared the PC prior to the conventional gamma prior for the shape parameter of the GE distribution under four different scenarios. These scenarios included– Setting 1: generating data from a linear setup and fitting a parametric model, Setting 2: generating data from a nonlinear setup and fitting a parametric model, Setting 3: generating data from a linear setup and fitting a semiparametric model, and Setting 4: generating data from a nonlinear setup and fitting a semiparametric model. For each setting, we used four different prior specifications: the PC prior with parameters 2.5 and 5 and the gamma prior with parameters (0.01, 0.01) and (1, 1). We compared their effectiveness in estimation. Additionally, we considered two cases for the number of samples, namely $n = 24$ and $n = 99$, to gain insights into parameter estimation in scenarios with small and large sample sizes, respectively. In each case of this simulation setup, we calculated the coverage probability of α based on 95% credible intervals and the absolute bias in estimating α to facilitate the comparison.

In the second simulation setup, we compared the efficiency of the semiparametric model with that of the parametric model. We considered four settings for this comparison– Setting 5: generating data from a linear setup and using a gamma prior for α , Setting 6: generating data from a linear setup and employing a PC prior for α , Setting 7: generating data from a nonlinear setup and using a gamma prior for α and finally, Setting 8: generating data from a nonlinear setup and employing a PC prior for α . We fitted the parametric and semiparametric models for each setting and compared their goodness of fit. We also examined variations in hyperparameters for each case. Specifically, in Settings 5 and 7, we considered the gamma prior with pa-

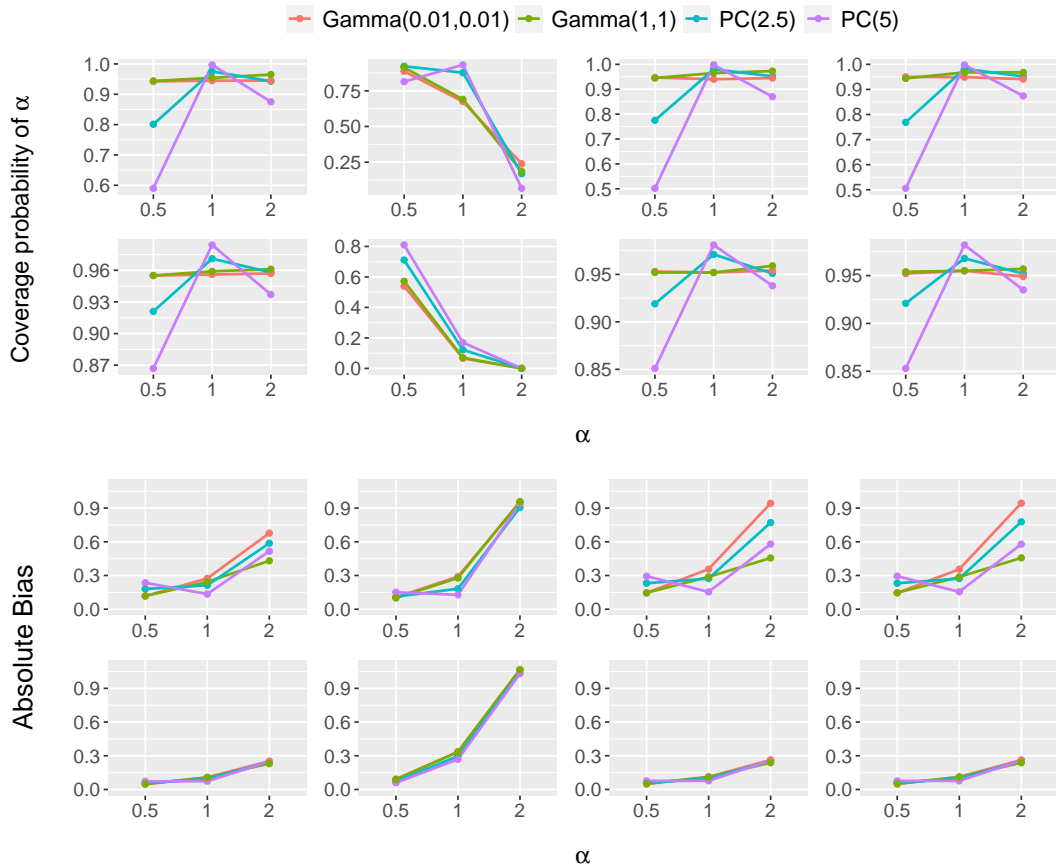


Figure 4. Coverage probabilities (top illustration) and absolute bias values (bottom illustration) computed based on imposing a PC prior. For each illustration, from the left-most to the right-most columns: (i) Setting 1 with $n = 24, 99$, (ii) Setting 2 with $n = 24, 99$, (iii) Setting 3 with $n = 24, 99$, (iv) Setting 4 with $n = 24, 99$.

rameters (0.01, 0.01) and (1, 1), respectively. In Settings 6 and 8, we employed the PC prior with parameters 2.5 and 5, respectively. Additionally, we explored two cases for the number of samples, namely $n = 24$ and $n = 99$, with the same objective as in the previous setup. In every case within this simulation setup, we have computed the absolute fitting error and the WAIC of the model fit with the estimated parameters as part of the comparison process.

All the simulations were conducted using three different values of α , the shape parameter: 0.5, 1, and 2. The choice of these values allowed us to explore various scenarios; the value of α being 1 represented the true scenario, resembling an exponential distribution. In contrast, the values of α being 0.5 and 2 indicated deviations from the exponential-like behavior. We utilized two different covariate sequences depending on the sample size. In (5), we assume $P = 1$ under all the simulation settings. When the sample size is $n = 24$, the covariate sequence we considered was $\mathbf{X} = (0.04, 0.08, \dots, 0.96)'$. For a larger sample size of $n = 99$, the covariate sequence was $\mathbf{X} = (0.01, 0.02, \dots, 0.99)'$. To generate data from the linear model, we constructed a design matrix with two columns: one for the intercept and the other for \mathbf{X} . However, for nonlinear data generation, we modified the second column of the design matrix to include $\sin(2\pi\mathbf{X})$ instead of \mathbf{X} . During fitting the parametric model, we used the same design matrix as the one employed during the linear data generation process when fitting the data. However, we introduced basis splines with ten basis functions

for the semiparametric setup. In total, we generated 1,000 datasets from the GE distribution. We employed MCMC techniques to deduce the parameters, utilizing 4,000 MCMC samples in total. The initial 2,000 samples were considered burn-in samples and excluded from analysis, while a thinning interval of 5 was applied.

Figure 4 corresponds to the first simulation setup. The coverage probabilities are the proportion of times the true value of α falls under the 95% credible intervals of α obtained from MCMC. The top illustration of Figure 4 presents the coverage probabilities of different simulation setups. Four columns represent Settings 1, 2, 3, and 4, with two rows representing sample sizes of 24 and 99, respectively. Each panel showcases four prior specifications represented by different lines, while the X-axis represents the different α values considered. In the bottom illustration of Figure 4, the identical simulation setups are depicted, but instead of coverage probabilities, it focuses on illustrating the absolute bias in the estimation of α .

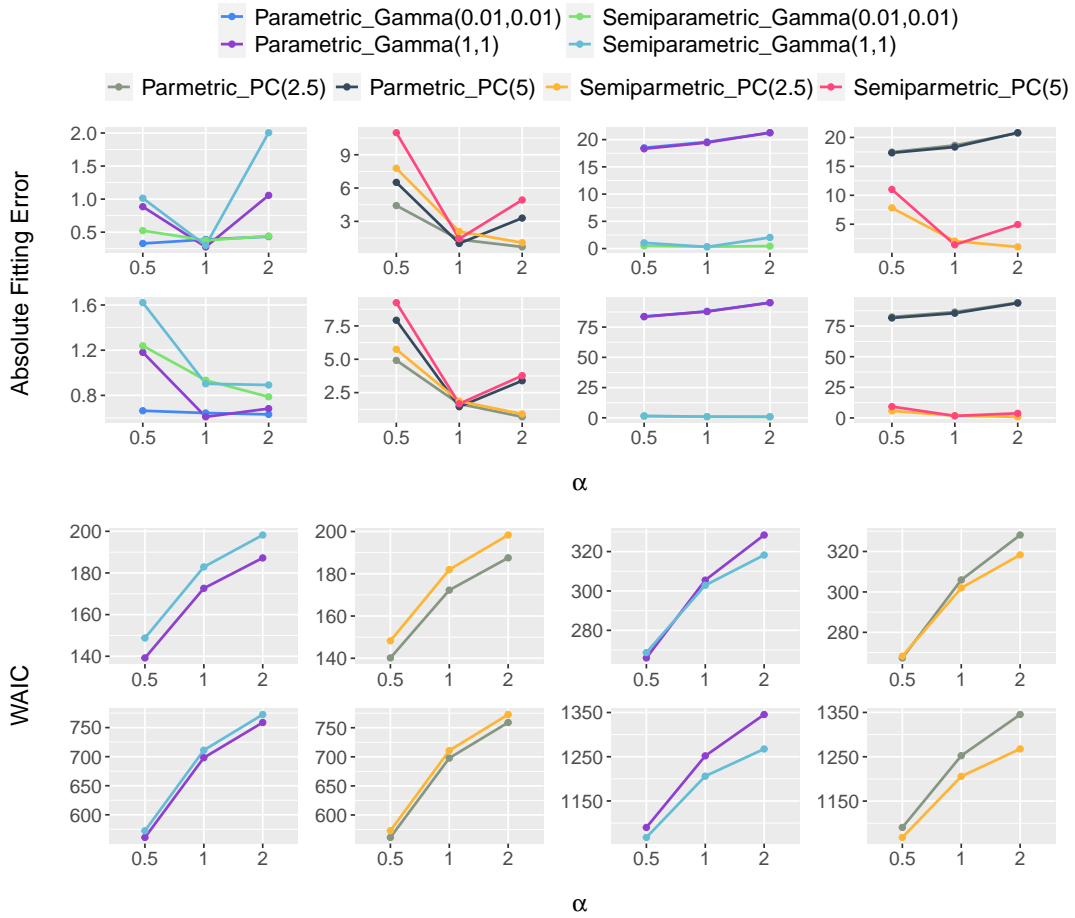


Figure 5. Absolute fitting error (top illustration) and WAIC values (bottom illustration) based on fitting a semiparametric GE regression model. For each illustration, from the left-most to the right-most columns: (i) Setting 5 with $n = 24, 99$, (ii) Setting 6 with $n = 24, 99$, (iii) Setting 7 with $n = 24, 99$, (iv) Setting 8 with $n = 24, 99$. (For the bottom illustration, the lines representing the gamma prior with parameters (0.01, 0.01) and the PC prior with $\theta = 5$ are excluded since they closely resemble the demonstrated prior specification).

Figure 5 focuses on the second simulation setup. In the top illustration of Figure 5, we compare the goodness of fit between the parametric and semiparametric models using the absolute fitting error. Similarly to previous figures, there are four columns representing Settings 5, 6, 7, and 8, with two rows representing sample sizes of 24

and 99. Each panel displays specifications of different values of α at the X-axis, and lines correspond to either the parametric setup or the semiparametric setup, with varying hyperparameter specifications. Moving to the bottom illustration of Figure 5, it provides a similar comparison but focuses on the WAIC of the model fit instead of the absolute fitting error.

The two aforementioned simulation steps offer substantial validation for the efficacy of the semiparametric regression setup and the utilization of the PC prior. The top illustration in Figure 4 clearly illustrates that when the true value of α approximates one, the PC prior exhibits superior coverage probability compared to the conventional gamma prior. This pattern holds across all four configurations in the initial simulation setup, except Setting 2, where both the gamma and PC priors yield undesirable outcomes due to attempts to fit a parametric linear model to highly non-linear data. Furthermore, the bottom illustration in Figure 4 highlights a reduction in estimation bias when α equals one, aligning with the inherent characteristic of the PC prior to shrink the estimate towards the base model. Additionally, the lower row within the same figure empirically confirms the well-established hypothesis that as the sample size increases, the influence of the prior gradually diminishes. This pattern is evident as the lines representing absolute bias nearly overlap, regardless of the chosen prior.

On the other hand, the top illustration in Figure 5 highlights a substantial increase in the absolute fitting error as we transition from a dataset demonstrating a linear trend to one illustrating a nonlinear trend. However, the plots associated with settings involving the generation of linear data and fitting a parametric model (Settings 5 and 6) exhibit minimal differences and occasionally yield superior results. When examining the settings where data originates from a nonlinear context (Settings 7 and 8), a distinct and considerable gap emerges between the lines representing the parametric and semiparametric models, where the latter consistently performs less favorably than the former, occupying a lower position on the graph. The lower illustration in Figure 5 conveys a similar observation. Despite Settings 5 and 6 pertaining to data generated from a linear setup, we observe that the parametric model consistently exhibits lower WAIC scores. In Settings 7 and 8, this ordering of WAIC scores is entirely reversed, with the lines representing the semiparametric model falling consistently below those of the parametric model. This reversal underscores the clear advantage of employing semiparametric modeling, particularly in scenarios characterized by high nonlinearity.

8. Data Application

We utilized the dataset introduced in Section 3 to drive our objective and conducted data analysis. The dataset comprises daily average rainfall for the wet days of the monsoon months during 1901–2022, focusing on Northern, Middle, and Southern Western Ghats regions. As outlined in Section 3, to account for the nonstationary nature of the dataset, we employed semiparametric regression techniques, using rainfall as the response variable and the corresponding year as the covariate. This analysis was performed separately for all three regions. With the validation from Section 3, we assumed the daily rainfall follows the GE distribution. Within a regression framework, we examined how the rate parameter of the GE distribution correlates with the covariate.

8.1. Model Description

We formulate our model such that the rate parameter of the GE distribution in the regression is influenced by the covariate ‘Year’ (T). Then, if Y_t represents our response variable of daily rainfall, our model is given as

$$Y_T|T = t \sim GE(\alpha, \lambda(t)) \text{ where } \lambda(t) \text{ is dependent on the covariate } T = t.$$

We conducted the analysis using two distinct models. The first model employs a parametric approach to model the rate parameter, while the second model is our proposed semiparametric formulation. We employed a simple linear regression model for the rate parameter in the parametric setting, given as $\lambda_{(L)}(t)$ in (9). On the other hand, for the semiparametric regression, we adopted the suggested basis spline regression form presented in (4). While Section 4.1 outlines the theory in a broader context, it is important to note that in practical application, we lack access to multiple covariate data. We have only one covariate (Year), and consequently, in this section, we take $P = 1$. With this, our model takes the form given as $\lambda_{(NL)}(t)$ in (9) given by

$$\lambda_L(t) = \exp(\beta_0 + \beta_1 t), \quad \lambda_{NL}(t) = \exp \left[\sum_{k=1}^K \beta_k B_k(t) \right]. \quad (9)$$

We employed Bayesian methods to estimate the model parameters. As the exploratory analysis shows a strong contraction of the considered GE distribution towards its base model, the exponential one, we used the proposed PC prior for the shape parameter α and chose independent flat Gaussian priors for the regression parameters. As discussed in Section [6], we resorted to the MCMC techniques to draw inferences about the model parameters.

We chose to utilize $K = 12$ basis functions for our analysis. With data spanning over 122 years, adopting 12 splines enabled us to capture decadal patterns using each spline effectively. To optimize the hyperparameter θ for the PC prior and achieve the most precise fit in our semiparametric regression, we computed WAIC values across a range of θ values, spanning within the interval $\{0.5, 1, \dots, 5\}$ for θ . After examining the northern, middle, and southern regions individually, we identified the optimal values for θ that yielded the lowest WAIC values. Specifically, for the Northern Western Ghats region, $\theta = 4.5$ demonstrated the most favorable outcome. Similarly, for the middle Western Ghats region, $\theta = 3.5$ was identified as optimal, while for the southern Western Ghats region, $\theta = 1.5$ exhibited superior performance. As a result, these chosen θ values were employed for their respective regions during the final model fitting stage.

We fitted six models corresponding to the two models and all three regions. For each of the model fits, we generated 10,000 MCMC samples for each model parameter. The initial 3,000 samples were removed as burn-in and subsequently excluded from the analysis. Additionally, we employed a thinning interval of 5. To evaluate convergence, mixing, and the behavior of the chains derived from the MCMC process, we visualize the trace plots of the parameters associated with both model fits in the supplementary materials. Specifically, we present the trace plots of the shape parameter α for each region. The regression parameters also exhibited similar satisfactory mixing behavior.

8.2. Model Comparison

In this section, we carry out a detailed comparison between the two model fits mentioned in (9). These model fits were obtained using a Bayesian approach through MCMC simulations, as elaborated upon in Section 8.1. The central focus of this comparison is visually represented in Figure 6. In this figure, we visually present the estimated mean daily rainfall on wet days for each year spanning the period from 1901 to 2022. These estimates are provided for the three regions separately, and both model fits – one characterized as semiparametric (depicted in red) and the other as parametric (depicted in blue). Furthermore, distinct panels are employed to illustrate various regions (the top panel represents the Northern region, the middle panel corresponds to the Middle region, and the bottom panel depicts the Southern region). In each panel, we display the estimated trajectory alongside a bar diagram, which offers a clear view of the annual average of daily rainfall on wet days for each year.

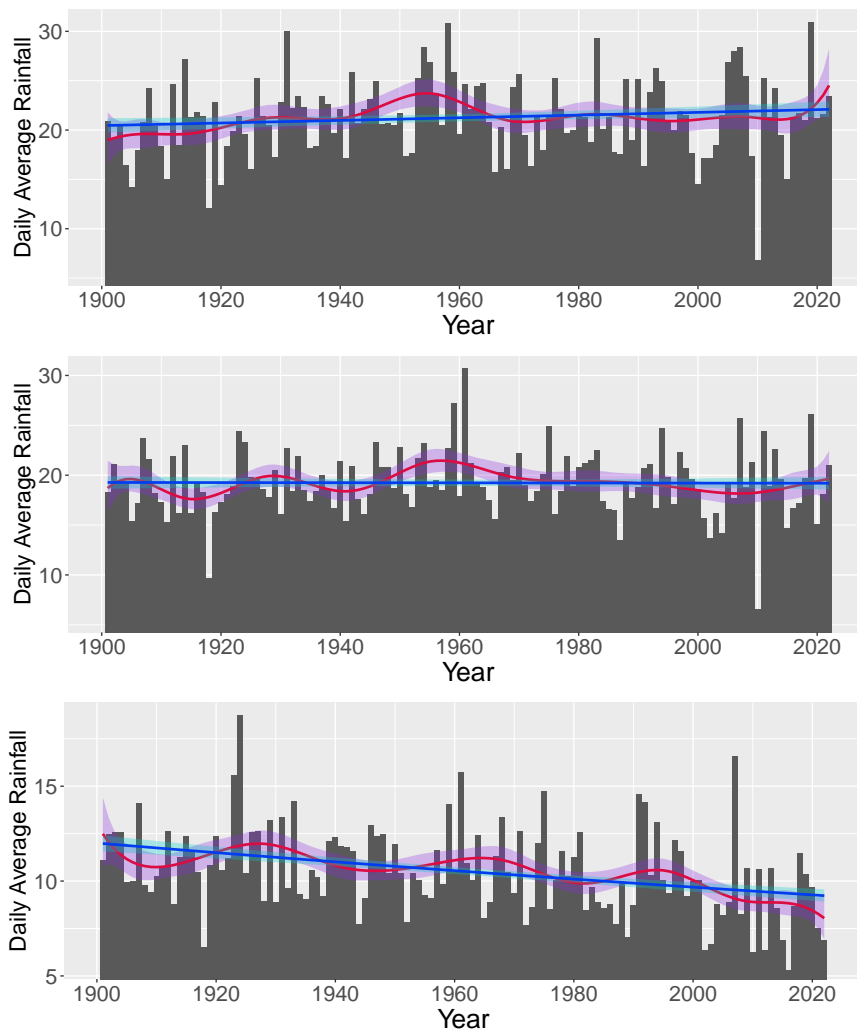


Figure 6. Estimated mean of daily wet-day rainfall (in mm) with Semiparametric (red line) and Parametric (blue line) models given by (9), along with corresponding point-wise 95% credible intervals (ribbons). The top, middle, and bottom panels show the results for the Northern, Middle, and Southern Western Ghats regions, respectively.

Across all three regions, a noticeable trend emerges: the semiparametric models ex-

hibit a notably superior fit. This distinction becomes evident as we observe multiple abrupt fluctuations in the bars representing the annual averages of wet-day precipitation. Remarkably, the semiparametric model effectively captures these fluctuations. Particularly noteworthy is the ability of the semiparametric model to accurately capture the nonstationarity present in the precipitation patterns. This heightened ability to encapsulate the dynamic variations in precipitation is a notable strength of the semiparametric model fitting. In Figure 6, we also provide a visual representation of a 95% credible interval for the trajectory, estimated from the MCMC samples. This interval allows us to understand the uncertainty associated with the estimation process.

8.3. Inferences about Western Ghats Rainfall

The fitted model offers valuable insights into the intricate short-term trends and features of rainfall in the Western Ghats region. Similar to the numerous instances in the literature where the authors modeled rainfall data using an exponential distribution [16, 46], our study also echoes this trend, aptly captured by the PC prior. The estimated GE shape parameters (posterior means) for the Northern, Middle, and Southern Western Ghats regions are 0.859, 0.949, and 0.873, respectively. Corresponding posterior standard deviations for these regions are 0.096, 0.100, and 0.097, respectively. These shape parameter values indicate a pronounced alignment with the exponential distribution of wet-day rainfall (the shape parameter is one). Consistent with the fluctuating pattern in the annual average of daily wet-day rainfall, the fitted mean lines for each region also demonstrate periodic crests and troughs. Besides, a consistent and stable mean rainfall trend is noticeable across the Northern and Middle Western Ghats regions. In the Southern Western Ghats region, the fitted parametric and semiparametric models distinctly reveal a decaying pattern in the annual averages of daily wet-day rainfall.

We present two significant insights into the rainfall patterns within these regions: the overarching decade-long shifts and individual region-specific probability rainfall plots. The calculation of the decadal change involves determining the overall rainfall shift and dividing it by the number of decades, resulting in $\{\mu(2022) - \mu(1901)\}/12.1$, where $\mu(t) = \lambda(t)^{-1} [\psi(\alpha + 1) - \psi(1)]$, and t representing the corresponding year. In this equation, α represents the estimated value of the shape parameter specific to the region, while $\lambda(t)$ denotes the fitted rate parameter values for the given year, t . Subsequently, the calculated decadal shifts in rainfall amount to 0.458 mm, 0.078 mm, and -0.367 mm for the northern, middle, and southern regions, respectively. In Figure 7, the probability rainfall graphs are displayed for three distinct probabilities: 0.3 (red line), 0.5 (blue line), and 0.7 (green line). In agrometeorology, 100 p % probability rainfall means the $(1 - p)^{th}$ quantile of the probability distribution of rainfall. These plots hold significant implications in agriculture as they empower farmers to formulate their harvesting strategies based on the anticipated likelihood of rainfall, allowing them to align their plans with the rainfall patterns to fulfill their specific requirements. Figure 7 showcases the estimated probability rainfall graphs, along with pointwise 95% credible intervals for the estimated rainfall. We derived these intervals from the MCMC samples; they illustrate the uncertainty associated with the estimation process.

As a crucial component of our comprehensive analysis, we further discuss the dynamic nature of annual average rainfall for the Western Ghats region over the past century by exploring the plot of its rate of change. Interpreting this quantity unveils insights into trends, variations, and shifts in mean values over time, offering glimpses

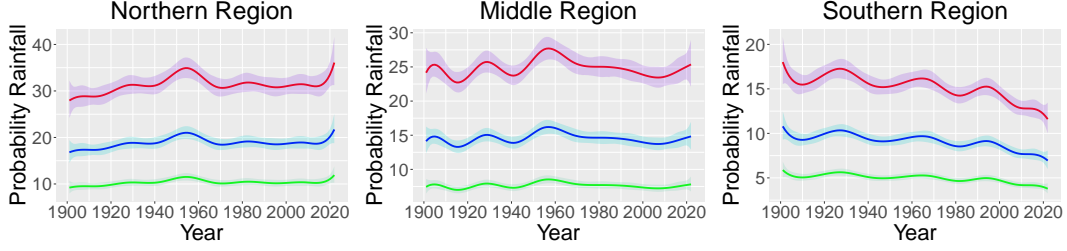


Figure 7. 30% (red line), 50% (blue line), and 70% (green line) probability rainfall (in mm) with corresponding point-wise 95% credible intervals (ribbons).

into rainfall behavior. A higher magnitude implies swift changes, while a lower one indicates gradual shifts. A positive rate denotes an increasing fitted mean rainfall over time, potentially signaling rising annual average rainfall. Conversely, a negative rate signifies a decreasing fitted mean, indicating a declining pattern and drier conditions. A rate of change near zero indicates a stable fitted mean rainfall. Fluctuations around zero imply short-term variations within a steady range. We compute this quantity by taking the derivative of the fitted mean from our semiparametric model with respect to the time component (t). This process involves differentiating the cubic B-splines from $\lambda_{NL}(t)$ in (9), given by

$$\frac{\partial\mu(t)}{\partial t} = -\frac{\psi(\alpha + 1) - \psi(1)}{[\lambda(t)]^2} \sum_{k=1}^K \beta_k \frac{\partial B_k(t)}{\partial t} \quad (10)$$

where we computed the derivatives of the cubic B-splines using `fda` package [37] in R. Figure 8 illustrates the plots depicting the rate of change over the years for each of the three regions (the left panel for the Northern region, the middle panel for the Middle region, and the right panel for the Southern region).

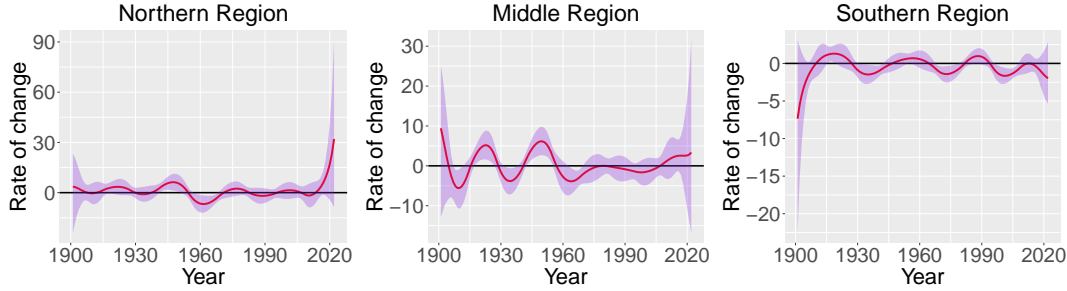


Figure 8. Rate of change in annual average of daily wet-day Rainfall in the monsoon months across the year 1920–2022, given by $\frac{\partial\mu(t)}{\partial t}$ in (10). The black line represents zero value.

For different regions of the Western Ghats mountain range, the data uncovers varying trends in rainfall patterns. Initially, the Northern and Middle regions exhibit more pronounced fluctuations in the rate-of-change graphs than the Southern region. This pattern suggests more rapid variations in rainfall trends in the Northern and Middle regions, while a more stable rainfall pattern is visible for the Southern area. Moreover, the small-scale positive and negative rate-of-change instances are well-balanced for the Northern and Middle regions. This pattern implies that over the past century, changes in rainfall have been relatively symmetric in terms of increase and decrease, with no significant alterations in long-term patterns. In contrast, the Southern re-

gion displays a substantial portion of years with graphs below the zero line, signifying a prevalent decreasing trend in rainfall. The rate-of-change in mean for the last 30 years shows consistent negative values in the Southern sector, indicating the declining rainfall trend, while the graphs for the other two regions consistently exhibit positive values, indicating an increasing trend in rainfall over the past three decades in those areas. The pointwise 95% credible intervals include the zero line for the Northern and Middle regions; hence, the positive values for the last years are not significant. On the other hand, while the posterior mean rate-of-change remains negative for the Southern region in general, the credible intervals indicate that the negative values of rate-of-change are significant for several timestamps; however, the positive values are generally insignificant.

9. Discussions and Conclusions

The Western Ghats, a formidable mountain range running parallel to the western coast of the Indian subcontinent, have a significant role in shaping precipitation patterns in Southern India. This impact is especially notable during the monsoon season, responsible for a substantial portion of the yearly rainfall of the region that is essential for ecosystem vitality and agricultural sustenance. The Western Ghats can be divided into Northern, Middle, and Southern regions. The proposed semiparametric generalized exponential (GE) regression model provides a reasonable fit for the wet-day rainfall data for all three regions. The model allows the marginal distributions to be the popular GE distribution.

With its shape and rate parameters, the GE distribution felicitates more rigorous skewness attributes than several other distributions. Thus, it is a better choice as a potential flexible model to incorporate high positive skewness in the data. Additionally, depending on the shape parameter, the varying nature of the hazard function provides GE distribution more compatibility in fitting into complex data structures. In the regression arena, semiparametric regression is a powerful statistical method that combines the flexibility of the nonparametric models with the interpretability and efficiency of the parametric models. The superiority of our proposed model in capturing nonlinearity compared to the corresponding parametric model is depicted in Sections 7 and 8. On the other hand, PC prior is a principled distance-based prior that penalizes departure from a base model and is used for specifying priors on parameters where it is difficult to elicit from expert knowledge directly. This paper introduces a PC prior for the shape parameter in the GE distribution, with the motivation of driving the GE distribution closer to the characteristics of the exponential distribution, a well-known probability distribution model for classical rainfall modeling.

There are several directions for extending this research. In addition to modeling the rate parameter, we can consider treating the shape parameter as a time-dependent variable. Instead of utilizing splines for the rate parameter, an alternative approach could involve employing a Gaussian process prior. Moreover, to ensure the applicability of our comparisons to large datasets, we may explore various approximation techniques like Gaussian Markov random fields [40]. While this paper has primarily focused on the temporal analysis of rainfall data, further enhancements can be made by incorporating spatial components [9]. This extension involves investigating the variability in rainfall patterns across diverse geographical regions or watersheds [54]. Additionally, there is potential for developing a real-time rainfall prediction system, offering timely information for tasks such as flood forecasting, reservoir management, and emergency

response, based on the foundation provided by this model. For the high-dimensional spatial problems, our model can be implemented as a two-stage model where the GE parameters can be estimated at each spatial location ignoring the spatial structure and those estimates can be smoothed using a Gaussian process [18].

From the application perspective, we observed a consistent overall trend with periodic fluctuations in the Northern and Middle Western Ghats regions. However, a clear declining trend was evident in the Southern Western Ghats region. This observation is further supported by the decadal analysis of rainfall changes in these three regions, where only the Southern region exhibited a clear and significant negative value indicating the effects of climate change. This research not only enhances our comprehension of the intricate climatic dynamics within the Western Ghats but also emphasizes the critical role of precise predictive models in anticipating seasonal rainfall variations.

Data availability statement

The dataset used in this paper can be downloaded (in a gridded data format) from https://www.imdpune.gov.in/cmpg/Griddata/Rainfall_1_NetCDF.html.

Disclosure statement

No potential conflict of interest was reported by the authors.

References

- [1] Abe, G. and James, E. (2013) Impacts of anthropogenic regulation on streamflow in the humid tropics of Western Ghat regions of Kerala state. *International Journal of Advances in Engineering & Technology* **6**(4), 1895.
- [2] Ahmad, Z., Hamedani, G. G. and Butt, N. S. (2019) Recent developments in distribution theory: a brief survey and some new generalized classes of distributions. *Pakistan Journal of Statistics and Operation Research* pp. 87–110.
- [3] Aslam, M. and Shahbaz, M. Q. (2007) Economic reliability test plans using the generalized exponential distribution. *Journal of Statistics* **14**(1), 53–60.
- [4] Cota-Felix, J. E., Rivas-Davalos, F. and Maximov, S. (2009) An alternative method for estimating mean life of power system equipment with limited end-of-life failure data. In *2009 IEEE Bucharest PowerTech*, pp. 1–4.
- [5] Dey, S. (2010) Bayesian estimation of the shape parameter of the generalised exponential distribution under different loss functions. *Pakistan Journal of Statistics and Operation Research* pp. 163–174.
- [6] Fahrmeir, L. and Lang, S. (2001) Bayesian semiparametric regression analysis of multi-categorical time-space data. *Annals of the Institute of Statistical Mathematics* **53**, 11–30.
- [7] Gelfand, A. E. and Kottas, A. (2003) Bayesian semiparametric regression for median residual life. *Scandinavian Journal of Statistics* **30**(4), 651–665.
- [8] Ghosal, S. and Van der Vaart, A. (2017) *Fundamentals of nonparametric Bayesian inference*. Volume 44. Cambridge: Cambridge University Press.
- [9] Gotway, C. A. and Stroup, W. W. (1997) A generalized linear model approach to spatial data analysis and prediction. *Journal of Agricultural, Biological, and Environmental Statistics* pp. 157–178.
- [10] Gupta, R. D. and Kundu, D. (1999) Theory & methods: Generalized exponential distributions. *Australian & New Zealand Journal of Statistics* **41**(2), 173–188.

- [11] Gupta, R. D. and Kundu, D. (2001a) Exponentiated exponential family: an alternative to gamma and Weibull distributions. *Biometrical Journal: Journal of Mathematical Methods in Biosciences* **43**(1), 117–130.
- [12] Gupta, R. D. and Kundu, D. (2001b) Generalized exponential distribution: different method of estimations. *Journal of Statistical Computation and Simulation* **69**(4), 315–337.
- [13] Gupta, R. D. and Kundu, D. (2007) Generalized exponential distribution: Existing results and some recent developments. *Journal of Statistical Planning and Inference* **137**(11), 3537–3547.
- [14] Hastie, T. J. and Tibshirani, R. J. (1990) *Generalized additive models*. Volume 43. Boca Raton: CRC press.
- [15] Hazra, A. (2022) Minimum density power divergence estimation for the generalized exponential distribution. *arXiv preprint arXiv:2206.08216* .
- [16] Hazra, A., Bhattacharya, S. and Banik, P. (2018) A Bayesian zero-inflated exponential distribution model for the analysis of weekly rainfall of the Eastern Plateau Region of India. *Mausam* **69**(1), 19–28.
- [17] Hazra, A. and Ghosh, A. (2019) Robust statistical modeling of monthly rainfall: The minimum density power divergence approach. *arXiv preprint arXiv:1909.08035* .
- [18] Hazra, A., Huser, R. and Jóhannesson, Á. V. (2021) Latent gaussian models for high-dimensional spatial extremes. *arXiv preprint arXiv:2110.02680* .
- [19] Hubert, M. and Vandervieren, E. (2008) An adjusted boxplot for skewed distributions. *Computational Statistics & Data Analysis* **52**(12), 5186–5201.
- [20] Jaheen, Z. F. (2004) Empirical Bayes inference for generalized exponential distribution based on records. *Communications in Statistics-Theory and Methods* **33**(8), 1851–1861.
- [21] Jorgensen, B. (1982) Statistical properties of the generalized inverse Gaussian distribution. *Lecture Notes in Statistics* **9**.
- [22] Kim, C. and Song, S. (2010) Bayesian estimation of the parameters of the generalized exponential distribution from doubly censored samples. *Statistical Papers* **51**, 583–597.
- [23] Koop, G. and Poirier, D. J. (2004) Bayesian variants of some classical semiparametric regression techniques. *Journal of Econometrics* **123**(2), 259–282.
- [24] Kullback, S. and Leibler, R. A. (1951) On information and sufficiency. *The Annals of Mathematical Statistics* **22**(1), 79–86.
- [25] Kundu, D. and Gupta, R. D. (2008) Generalized exponential distribution: Bayesian estimations. *Computational Statistics & Data Analysis* **52**(4), 1873–1883.
- [26] Kundu, D. and Raqab, M. Z. (2005) Generalized Rayleigh distribution: different methods of estimations. *Computational Statistics & Data Analysis* **49**(1), 187–200.
- [27] Lee, J. and Sison-Mangus, M. (2018) A Bayesian semiparametric regression model for joint analysis of microbiome data. *Frontiers in Microbiology* **9**, 522.
- [28] Li, L. and Hanson, T. E. (2014) A Bayesian semiparametric regression model for reliability data using effective age. *Computational Statistics & Data Analysis* **73**, 177–188.
- [29] Madi, M. T. and Raqab, M. Z. (2007) Bayesian prediction of rainfall records using the generalized exponential distribution. *Environmetrics* **18**(5), 541–549.
- [30] Markiewicz, I., Strupczewski, W. G., Bogdanowicz, E. and Kochanek, K. (2015) Generalized exponential distribution in flood frequency analysis for Polish rivers. *PloS One* **10**(12), 1–26.
- [31] Marshall, A. W. and Olkin, I. (1997) A new method for adding a parameter to a family of distributions with application to the exponential and Weibull families. *Biometrika* **84**(3), 641–652.
- [32] Mathew, M. M., Sreelash, K., Mathew, M., Arulbalaji, P. and Padmalal, D. (2021) Spatiotemporal variability of rainfall and its effect on hydrological regime in a tropical monsoon-dominated domain of Western Ghats, India. *Journal of Hydrology: Regional Studies* **36**, 100861.
- [33] Naqash, S., Ahmad, S. and Ahmed, A. (2016) Bayesian analysis of generalized exponential distribution. *Journal of Modern Applied Statistical Methods* **15**(2), 38.

- [34] Nguyen-Huy, T., Deo, R. C., Mushtaq, S. and Khan, S. (2020) Probabilistic seasonal rainfall forecasts using semiparametric d-vine copula-based quantile regression. In *Handbook of Probabilistic Models*, pp. 203–227. Elsevier.
- [35] Ordoñez, J. A., Prates, M. O., Bazán, J. L. and Lachos, V. H. (2023) Penalized complexity priors for the skewness parameter of power links. *Canadian Journal of Statistics (Published online)*.
- [36] Rajeevan, M., Bhate, J. and Jaswal, A. K. (2008) Analysis of variability and trends of extreme rainfall events over India using 104 years of gridded daily rainfall data. *Geophysical Research Letters* **35**(18).
- [37] Ramsay, J. (2023) *fda: Functional Data Analysis*. R package version 6.1.4.
- [38] Raqab, M. Z. and Madi, M. T. (2005) Bayesian inference for the generalized exponential distribution. *Journal of Statistical Computation and Simulation* **75**(10), 841–852.
- [39] Reich, B. J. and Ghosh, S. K. (2019) *Bayesian statistical methods*. Boca Raton, USA: CRC Press.
- [40] Rue, H. and Held, L. (2005) *Gaussian Markov random fields: theory and applications*. CRC press.
- [41] Rue, H., Martino, S. and Chopin, N. (2009) Approximate Bayesian inference for latent Gaussian models by using integrated nested Laplace approximations. *Journal of the Royal Statistical Society: Series B (Statistical Methodology)* **71**(2), 319–392.
- [42] Sarhan, A. M. (2007) Analysis of incomplete, censored data in competing risks models with generalized exponential distributions. *IEEE Transactions on Reliability* **56**(1), 132–138.
- [43] Simpson, D., Rue, H., Riebler, A., Martins, T. G. and Sørbye, S. H. (2017) Penalising model component complexity: A principled, practical approach to constructing priors. *Statistical Science* **32**(1), 1–28.
- [44] Sørbye, S. H. and Rue, H. (2017) Penalised complexity priors for stationary autoregressive processes. *Journal of Time Series Analysis* **38**(6), 923–935.
- [45] Tahir, M. H. and Cordeiro, G. M. (2016) Compounding of distributions: a survey and new generalized classes. *Journal of Statistical Distributions and Applications* **3**, 1–35.
- [46] Todorovic, P. and Woolhiser, D. (1974) Stochastic model of daily rainfall. *Miscellaneous Publication, US Department of Agriculture* **1275**, 232 – 246.
- [47] Van Niekerk, J., Bakka, H. and Rue, H. (2021) A principled distance-based prior for the shape of the Weibull model. *Statistics & Probability Letters* **174**, 109098.
- [48] Varikoden, H., Revadekar, J., Kuttippurath, J. and Babu, C. (2019) Contrasting trends in southwest monsoon rainfall over the Western Ghats region of India. *Climate Dynamics* **52**, 4557–4566.
- [49] Veerabhadranavar SA, V. B. (2022) Assessment of Impact of Climate Change in the Western Ghats Region, India. *Indian Journal of Science and Technology* pp. 1466–1472.
- [50] Venkatesh, B., Nayak, P., Thomas, T., Jain, S. K. and Tyagi, J. (2021) Spatio-temporal analysis of rainfall pattern in the Western Ghats region of India. *Meteorology and Atmospheric Physics* **133**, 1089–1109.
- [51] Ventrucci, M. and Rue, H. (2016) Penalized complexity priors for degrees of freedom in Bayesian p-splines. *Statistical Modelling* **16**(6), 429–453.
- [52] Watanabe, S. and Opper, M. (2010) Asymptotic equivalence of Bayes cross validation and widely applicable information criterion in singular learning theory. *Journal of Machine Learning Research* **11**, 3571–3594.
- [53] Wigena, A. H., Djuraidah, A. and Rizki, A. (2015) Semiparametric modeling in statistical downscaling to predict rainfall. *Applied Mathematical Sciences* **9**(88), 4371–4382.
- [54] Yang, C., Chandler, R., Isham, V. and Wheeler, H. (2005) Spatial-temporal rainfall simulation using generalized linear models. *Water Resources Research* **41**(11).

Appendix A Kullback-Leibler divergence between generalized exponential (GE) and exponential distribution

The density function of a random variable following a GE distribution with shape parameter α and rate parameter λ is given by $f(y) = \alpha\lambda (1 - e^{-\lambda y})^{\alpha-1} e^{-\lambda y}$, $y > 0$, and that of a random variable following an exponential distribution with rate parameter λ is given as $g(y) = \lambda e^{-\lambda y}$, $y > 0$. Thus, the KLD between the GE distribution and the exponential distribution can be obtained as

$$\begin{aligned}
\text{KLD}(f \parallel g) &:= \text{KLD}(\alpha) \\
&= \int_0^\infty \log\left(\frac{f(y)}{g(y)}\right) \cdot f(y) dy \\
&= \log(\alpha) \int_0^\infty f(y) dy + (\alpha - 1) \int_0^\infty \log(1 - e^{-\lambda y}) \cdot f(y) dy \\
&= \log(\alpha) + (\alpha - 1) \int_0^\infty \log(1 - e^{-\lambda y}) \cdot \alpha\lambda (1 - e^{-\lambda y})^{\alpha-1} e^{-\lambda y} dy \\
&= \log(\alpha) - (\alpha - 1) \int_0^\infty \alpha x \cdot e^{-x(\alpha-1)} \cdot e^{-x} dx \quad \left[\text{replacing } e^{-x} = 1 - e^{-\lambda y} \right] \\
&= \log(\alpha) + \frac{(1 - \alpha)}{\alpha}.
\end{aligned}$$